THE JOURNAL OF PHYSICAL CHEMISTRY Letters

pubs.acs.org/JPCL

Letter

Quantification of the Structure of Colloidal Gas–Liquid Interfaces

Mark Vis,* Kelly J. H. Brouwer, Álvaro González García, Andrei V. Petukhov, Oleg Konovalov, and Remco Tuinier

Cite This: J. Phys. Chem. Lett. 2020, 11, 8372–8377

Read Online

ACCESS | Metrics & More | Article Recommendations | Supporting Information

ABSTRACT: We have quantified the structure of the colloidal gas–liquid interface using synchrotron X-ray reflectivity measurements on a model colloid–polymer mixture. The interfacial width shows mean-field scaling with the colloid density difference, and the density profiles appear to be monotonic. Furthermore, our measurements allow us to distinguish between different theoretical polymer descriptions commonly used to model colloid–polymer mixtures. Our results highlight the importance of capturing the correct polymer physics in obtaining a quantitative theoretical description of the colloidal gas–liquid interface.

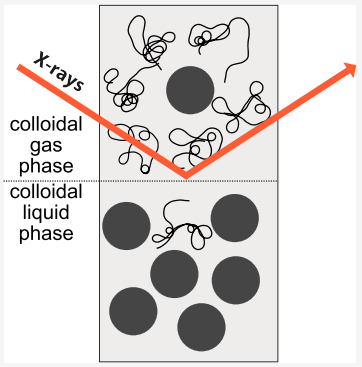

Through computer simulations[1,2] and experiments[3] it has been rigorously established that dispersions of colloidal hard spheres (HSs) undergo an entropy-driven phase transition from a fluid phase to a crystal phase at a sufficiently high density. Reminiscent of atomic systems,[4−6] colloidal spheres may also display a gas–liquid critical point if the particles additionally exhibit sufficiently strong and long-range mutual attractions.[7]

One way to generate well-defined attractions in colloidal systems is through addition of nonadsorbing polymers.[8−11] The configurational entropy of polymer chains is reduced in a region near a colloidal surface,[8] the so-called depletion zone. Therefore, when two colloidal particles approach and their depletion zones overlap, the free volume for the nonadsorbing polymer increases, and hence, their configurational entropy increases too. The colloidal particles therefore experience an effective attraction. The strength of this attraction can be manipulated by varying the polymer concentration, whereas its relative range is set by the polymer-to-colloid size ratio $q = 2R_g/d$, where R_g is the radius of gyration of the polymer and d is the diameter of the colloidal spheres. Typically, a colloidal gas–liquid critical point exists for $q \gtrsim 1/3$.[11−13]

This depletion interaction is often used as an adequate tool to induce attractions between repulsive model colloids to mimic molecular systems at more accessible length and time scales. Such systems may be regarded as supramolecular "designer atoms" interacting through a Lennard-Jones-like combination of a short-range repulsion and a long-range attraction.[4,14] However, the abundance of colloidal particles in complex multicomponent mixtures featuring a wide range of interactions, ranging from food products to paints,[15−19] highlights the fundamental importance of depletion attractions and related phase transitions driven by excluded-volume interactions of added compounds, especially since such systems are not direct analogues of molecular mixtures.

Here we focus on the interface between coexisting colloidal gas and liquid phases. Interfaces in colloidal systems hold many surprising features because of the different length scales involved.[20] The interfacial tension $\gamma \sim k_BT/d^2$, where k_BT is the thermal energy, is at least 3–6 orders of magnitude smaller than for molecular systems, even bringing colloidal thermal capillary waves[21−23] into reach of optical techniques.[24] Comparable interfaces exist in related systems, such as aqueous two-phase systems,[25] and hence, understanding their fundamental physics is a key challenge for practical applications such as water-in-water emulsions.[26]

Given the fascinating properties of colloidal gas–liquid interfaces, it is surprising that there have been limited studies concerning the characteristics that essentially *define* the interface: the density profiles and associated widths. Brader and Evans[27] have shown, modeling the polymers as penetrable hard spheres (PHSs) and using a van der Waals-like approach, that these interfaces have a width comparable to the colloid size. The description of polymers as PHSs in colloid–polymer mixtures is also known as the AOV model,[8,10] where the polymers are modeled as spheres that can freely overlap each

Received: August 12, 2020
Accepted: September 15, 2020
Published: September 21, 2020

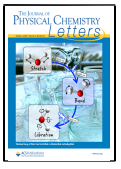

other but cannot overlap the colloids. Using density functional theory, Brader et al.[28] later showed that the profiles may feature layering, i.e., density profiles that decay in an oscillatory fashion far from the critical point, similar to the surfaces of liquid metals.[29] Although some experiments have been reported on this subject,[30,31] it is surprising that these predictions have not yet been subject to systematic quantitative scrutiny.

In this work we present a systematic quantification of colloidal gas−liquid interfaces in a model colloid−polymer mixture using X-ray reflectivity (XRR) for various points in the phase diagram. XRR allows us to reach much smaller length scales than, for instance, optical microscopy while simultaneously providing statistical averaging over large sample areas (several centimeters). Reaching nanometer interfacial resolution is highly relevant for various practical systems, such as those mentioned previously, which have length scales beyond the reach of optical techniques; therefore, we believe that it is crucial to apply XRR to colloidal systems.

In theoretical descriptions of colloid−polymer mixtures, various models for the polymeric depletants have been employed, including the aforementioned PHS model. Experimentally assessing the accuracy of these various models is therefore of particular interest in this work. To this end, we employ sterically stabilized silica spheres[32−34] with $d = 29.4 \pm 2.2$ nm dispersed in cyclohexane, which behave essentially as hard spheres.[35] These particles are mixed with polydimethylsiloxane (PDMS) with molar mass $M_w = 117$ kg mol^{-1} and $R_g \approx 16.4$ nm in cyclohexane (a good solvent for PDMS), and thus, $q \approx 1.1$. After mixing at appropriate concentrations, the mixture shows gas−liquid phase separation into a colloid-poor top phase and a colloid-rich bottom phase. Our XRR experiments were carried out at the European Synchrotron Radiation Facility in Grenoble, France, on ID10[36] in home-built sample cells using a one-dimensional detector (parallel to the interface, K_y direction) under specular conditions (equal grazing and detector angles θ, K_z direction). The cell height is comparable to the gravitational length of the particles, and thus, effects of sedimentation are minimized. For more details, the reader is referred to the Supporting Information (SI).

Scanning the detector and grazing angle θ simultaneously during an XRR experiment yields data such as exemplified in Figure 1. Here the bright vertical streak represents the specularly reflected X-ray beam, which sits on a background dominated by the form and structure factor of the colloidal liquid phase. It should be noted that because of the limited contrast and relatively large interfacial length scale, the relevant detection angles are rather small ($\theta < 0.1°$).

After background subtraction (see the SI), the reflected intensity as a function of $K_z = (4\pi/\lambda) \sin\theta$, where λ is the wavelength of the incident beam and θ is the angle between the beam and the interface, is shown in Figure 2 (data points) for samples with varying polymer concentrations.[37]. At tiny values of K_z (~0.01 nm^{-1}), the direct beam is detected, which is used to normalize the intensities. Following an initial drop as the direct beam is moved away from the detector, the intensity starts to increase for slightly larger K_z values because of specular reflection. Since the footprint of the X-ray beam is initially larger than the sample (i.e., it spills over the sample area) and becomes smaller with increasing angle, in this regime the intensity increases with K_z. Additionally, other effects such as possible disturbances by menisci or large-scale undulations of the surface, which may differ for each sample because of

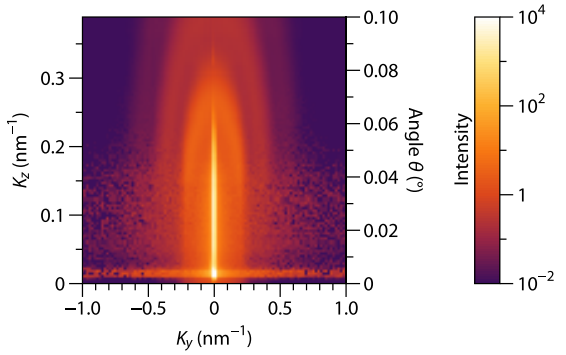

Figure 1. Example of an X-ray reflectivity density plot for a colloidal gas−liquid interface in a sample consisting of 141 g L^{-1} colloidal silica spheres ($d = 29.4 \pm 2.2$ nm) and 31.5 g L^{-1} nonadsorbing polymer (PDMS, 117 kg mol^{-1}, $R_g \approx 16.4$ nm). Colors indicate reflected intensity on a logarithmic scale (see the legend, arb. units). The bright vertical streak represents the specularly reflected beam, whereas the background is dominated by bulk scattering of the colloidal liquid phase.

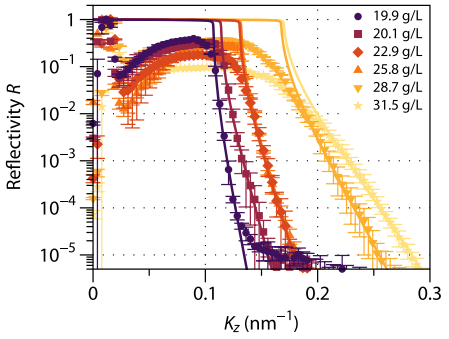

Figure 2. X-ray reflectivity of colloidal gas−liquid interfaces as a function of the polymer concentration for a fixed colloidal silica concentration of 141 g L^{-1}. Data points represent experimental values, and solid curves are theoretical fits.

differing capillary lengths, are reduced when the angle θ is increased. Next, there is a sharp decrease in the reflected intensity above a critical angle. For reflectivities $R \lesssim 10^{-5}$, the reflected beam can no longer be separated from scattering.

The experimental data are modeled as follows. For electromagnetic waves reflecting from a perfectly flat and sharp interface, the coefficient of the reflected amplitude, $r_F(\theta) \equiv A_r/A_{in}$, is given by[38]

$$r_F(\theta) = \frac{\sin\theta - \sqrt{\left(\frac{n_b}{n_t}\right)^2 - \cos^2\theta}}{\sin\theta + \sqrt{\left(\frac{n_b}{n_t}\right)^2 - \cos^2\theta}} \quad (1)$$

where n_b and n_t are the refractive indices of the bottom and top phases, respectively, which may have an imaginary part to account for absorption. For X-rays, n_j is usually expressed in terms of the parameters δ and β as $n_j = 1 - \delta_j - i\beta_j$. The reflected intensity follows as the absolute square of the reflected amplitude. This defines the so-called Fresnel reflectivity of a flat interface, $R_F(\theta) = |r_F(\theta)|^2$. A critical angle is commonly defined as $\cos\theta_c = n_b/n_t$. In the case of negligible absorption ($\beta = 0$), for $\theta \leq \theta_c$ the interface shows total external reflection of X-rays.

https://dx.doi.org/10.1021/acs.jpclett.0c02464
J. Phys. Chem. Lett. 2020, 11, 8372−8377

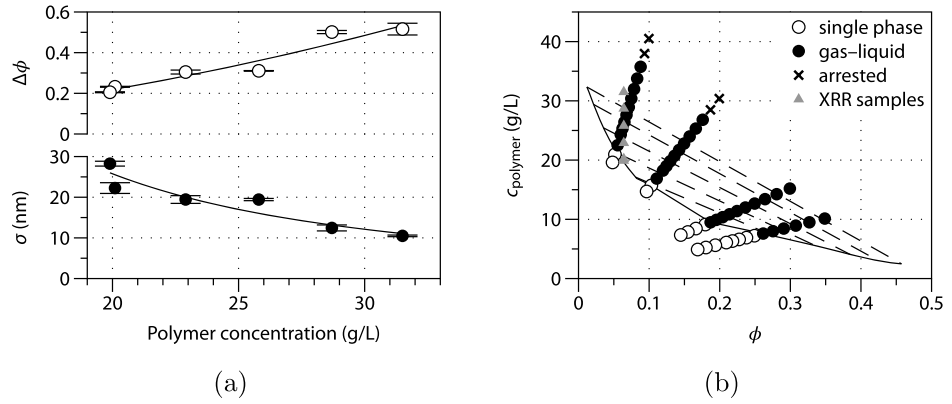

Figure 3. (a) Gas−liquid colloid volume fraction difference $\Delta\phi$ and interfacial width σ as functions of the concentration of nonadsorbing polymer resulting from the fits shown in Figure 2. The curves are to guide the eye; the error bars indicate the standard deviations from multiple measurements on the same sample. (b) Phase diagram of the system determined according to the method of Bodnár and Oosterbaan,[39] where the solid curve is the binodal and some representative tie lines are dashed.

There are various approaches to model interfaces that are diffuse rather than sharp. Arguably one of the simplest models for a diffuse interface that is often used in XRR is obtained through incorporation of the so-called Croce−Névot factor.[38] This model assumes that the interfacial profile follows a cumulative normal/Gaussian distribution (given by the error function), where σ is the width (that is, the standard deviation) of the normal distribution. Naturally, σ is not *the* width of the interface but merely a *measure* for the width. In the literature various other measures for the interfacial width exist, such as the so-called "10−90% width" W_{10-90}.[27] It is trivial to show that $W_{10-90} \approx 2.6\sigma$ for an interface following a (cumulative) normal distribution (also see the SI). The Croce−Névot factor is given by

$$r_\sigma(\theta) = \exp\left[-2\sigma^2\left(\frac{2\pi}{\lambda}\right)^2 \sin\theta \sqrt{\left(\frac{n_b}{n_t}\right)^2 - \cos^2\theta}\right] \quad (2)$$

and describes the change in the reflected amplitude due to the Gaussian diffuseness σ. Thus, in this model the reflectivity of a rough interface is

$$R(\theta) = |r_F(\theta) r_\sigma(\theta)|^2 \quad (3)$$

It should be stressed that the width σ essentially collects all sources of interfacial "diffuseness", be they due to so-called intrinsic density profiles or thermal fluctuations of the interfacial position (i.e., capillary waves). To separate these contributions experimentally requires off-specular measurements, which were beyond the scope of this work.

When describing our data with eq 3, there are two fitting parameters. First, the contrast factor n_b/n_t is unknown, since the compositions of the two coexisting phases are not exactly known beforehand. The contrast factor is directly related to the volume fraction difference between the colloidal liquid and gas phases, $\Delta\phi = \phi^l - \phi^g$, since the polymer and solvent have essentially the same contrast for X-rays and the polymer concentration is rather low (see the SI for more details). The colloid density difference $\Delta\phi$ serves as a measure of the distance to the critical point. The second fit parameter is the Gaussian interfacial width σ. Both the colloid density difference $\Delta\phi$ and width σ, as apparent from fits to the reflectivity data, are plotted in Figure 3a as functions of the polymer concentration. With increasing polymer concentration, the distance to the critical point becomes larger, as can also be seen in the phase diagram in Figure 3b. As a result, the density difference $\Delta\phi$ goes up while the width σ goes down. In our studied region, relatively far from the critical point, the width is at most equal to the colloid size.

Next, we compare our experimental results to theoretical predictions made by generalized free-volume theory (GFVT) to test various polymer descriptions often employed for colloid−polymer mixtures. Although GFVT describes the *bulk* phase behavior of model colloid−polymer mixtures in a physical and accurate way,[11,40] this does not guarantee correct predictions of the interfacial structure—in fact, this aspect has hardly been tested. The interfacial properties are here predicted using a van der Waals-like approach.[41,42]

Within GFVT, the dimensionless semigrand potential of the colloid−polymer mixture, $\tilde{\Omega} = \Omega v_c/(k_B T V)$, where $v_c = \pi d^3/6$ is the colloid volume, $k_B T$ is the thermal energy, and V is the volume, is given by

$$\tilde{\Omega} = \tilde{F}_0 - q^{-3} \int_0^{\phi_d^R} \mathrm{d}\phi_d^{R'} \left(\frac{\partial \tilde{\Pi}_d^R}{\partial \phi_d^{R'}}\right) \alpha(\phi_d^{R'}) \quad (4)$$

for a system in equilibrium with a reservoir (R) of constant polymer volume fraction ϕ_d^R. The first term on the right-hand side is the free energy of a polymer-free hard-sphere fluid, given by the Carnahan−Starling equation,[43] and the second term represents the change in free energy due to addition of the polymer. The latter follows from the free volume fraction α—which denotes the (normalized) part of the system volume that is accessible to the polymer chains and generally depends on the polymer and colloid volume fractions and the size ratio—and the polymer osmotic pressure $\tilde{\Pi}_d^R$. Scaling relations for the effective depletion zone size and polymer osmotic pressure with polymer concentration essentially describe the physics of the depletant (see the SI). These scaling relations can take into account shrinkage of depletion zones by osmotic compression at large ϕ_d^R *and* by configurations of polymer chains around spherical colloids at large q. Here we focus on three specific models to account for the polymer chains in describing HSs plus polymer mixtures, namely, PHS (i.e., ideal polymers or the AOV model[8−10]), polymers in theta solvent, and polymers in good solvent.[40] It should be noted that for the PHS scenario, GFVT reduces to the simpler free-volume theory (FVT).[12]

https://dx.doi.org/10.1021/acs.jpclett.0c02464
J. Phys. Chem. Lett. 2020, 11, 8372−8377

By the use of the above ingredients, phase equilibria may be computed using standard thermodynamics. We may now also compute interfacial properties. Let $\tilde{W}(\phi)$ express the variation of the free energy along a colloidal gas−liquid interface, such that[41,42]

$$\tilde{W}(\phi) = \tilde{\Omega}(\phi) - \phi\tilde{\mu}_{eq} + \tilde{\Pi}_{eq} \quad (5)$$

where $\tilde{\mu}_{eq}$ is the colloid chemical potential and $\tilde{\Pi}_{eq}$ is the osmotic pressure in each of the two coexisting phases. Within the square-gradient approximation, the tension of the gas−liquid interface reads as

$$\tilde{\gamma} \equiv \frac{(\pi/6)^{3/2} d^2}{k_B T}\gamma = 2\int_{\phi^g}^{\phi^l} \sqrt{\tilde{m}\tilde{W}(\phi)}\, \mathrm{d}\phi \quad (6)$$

where ϕ^g and ϕ^l are the coexisting colloid volume fractions and $\tilde{m}$ is the second moment of the direct correlation function $c(\tilde{r})$, which we assume follows from the colloid−colloid pair potential (see the SI). The interfacial colloid density profiles may be evaluated numerically via

$$-\tilde{W}(\phi) + \tilde{m}\left(\frac{\mathrm{d}\phi}{\mathrm{d}z}\right)^2 = 0 \quad (7)$$

where z is the perpendicular distance from the interface, where we define $z = 0$ from the condition $\phi(z = 0) = (\phi^g + \phi^l)/2$. In eq 7, small values of $\tilde{m}$ favor sharper interfaces and larger values favor broader interfaces.

Using this approach, we calculated colloid density profiles based on GFVT for the experimental value of $q = 1.1$ for various polymer concentrations and models. Figure 4 shows an example for the scenario of polymers under good solvent conditions. We emphasize here the use of the colloid density difference $\Delta\phi$ for comparisons to the experiments, since this parameter is accessible both experimentally and theoretically and gives an absolute measure of the distance to the critical point.

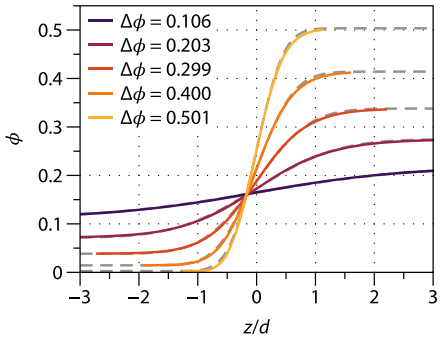

Figure 4. Colloid density profiles (solid curves) as calculated using generalized free-volume theory for polymers in a good solvent and corresponding Gaussian fits (dashed curves) with σ/d = 2.09, 1.08, 0.71, 0.51, and 0.37 for the indicated values of the colloid density difference $\Delta\phi$ (top to bottom).

In analyzing experimental data, we assumed a Gaussian diffuseness of the interface, i.e., density profiles described by a cumulative normal distribution (error function). We therefore fitted the profiles in Figure 4 to a cumulative normal distribution of width σ, shown as the dashed curves, to quantify the widths in a fashion that enables a direct comparison with the results from the analysis of the XRR experiments (see also eq S10 in the SI). The profiles are well-described by this approach. We note that other approaches to quantify the width yield essentially the same results (see Figure S7a).

Figure 5 compares the interfacial width σ as a function of the colloid volume fraction difference $\Delta\phi$ as obtained experimentally (points) and theoretically for $q = 1.1$ (curves). The PHS model utilized by FVT shows good agreement with experiments at small $\Delta\phi$ values of ∼0.2 to 0.3 but an unphysical *increase* in the interfacial width further from the critical point that is not seen in the experiments. We believe this to be connected to the unusually high PHS concentrations required to reach a large $\Delta\phi$ for the colloids, originating from the broad liquid window of the PHS model[40,44] (also see the calculated phase diagram in Figure S5). Through strongly attractive pair potentials, this leads to large values of $\tilde{m}$, favoring broader interfaces on the basis of eq 7.[45] The PHS model is popular in describing experimental colloid−polymer mixtures with small q and can give (semi)quantitative agreement with respect to the bulk phase behavior,[11] yet here we see that for interfacial purposes it is qualitatively inaccurate in the FVT framework, at least at these relatively large q values.

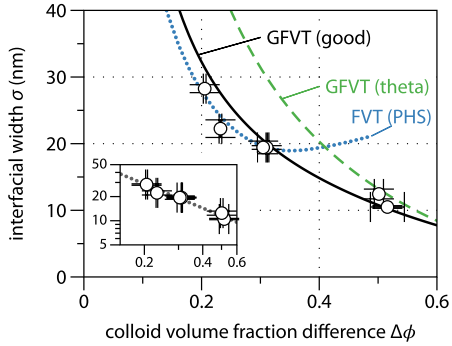

Figure 5. Interfacial width σ as a function of the colloid gas−liquid density difference $\Delta\phi$ from X-ray reflectivity measurements (data points) and from free-volume theory (curves) using the penetrable hard sphere (PHS), polymers in theta solvent (theta), and polymers in good solvent (good) polymer models. As a reference, the mean-field scaling ($\sigma \propto \Delta\phi^{-1}$) is shown (inset, dotted line). The error bars indicate the standard deviations from multiple measurements on the same sample.

GFVT combined with a model for polymers in a theta solvent, on the other hand, significantly overestimates the interfacial width closer to the critical point, although it matches better far from the critical point. When describing the polymers using GFVT in a good solvent, quantitative agreement between experiment and theory over the full range is found. Importantly, this model also quantitatively describes the interfacial tension as measured by others for a similar system (see Figure S7b). Remarkably, no fitting parameters are involved in achieving this agreement; we merely set the colloid diameter d and size ratio q to their experimental values. These results highlight that the precise scaling laws of the polymer at hand, including solvency effects, and other approximations made, are of great consequence for the structure of colloidal gas−liquid interfaces. Additionally, we find that $\sigma \propto \Delta\phi^{-1}$ (see the inset) in the region of $\Delta\phi$ accessible here, which is relatively far from the critical point.

The agreement between our experiments and GFVT, which contains mean-field approximations, may raise questions

https://dx.doi.org/10.1021/acs.jpclett.0c02464
J. Phys. Chem. Lett. 2020, 11, 8372−8377

regarding the role of thermal capillary waves.[24] A possibility is that our experiments are less sensitive to capillary waves because of the finite slit size of the detector.[46] Also, the bending rigidity of the interface may play a role in the manifestation of the waves.[22] It must also be noted that separating the interfacial width into contributions of "intrinsic" profiles and capillary waves is not trivial at best.[47] Still, one may expect the capillary waves only to broaden the GFVT profiles. Further work is required to shed light on this matter.

Capillary waves may also be responsible[48] for diminishing the magnitude of the oscillations in the density profiles revealed from the DFT approach of Brader and co-workers.[28] Such oscillations, which are predicted to exist only far from the critical point and to have a period of about $0.9d$, should yield a pronounced and positive deviation from the exponential decay of the reflectivity at $K_z \approx 2\pi/(0.9d) \approx 0.24$ nm^{-1} (see Figure S4, black dotted curve). Such deviations are not evident from the results in Figure 2.

In conclusion, we have probed the structure of a model colloidal gas−liquid interface using synchrotron X-ray reflectivity. Our results indicate that a realistic treatment of the polymer physics, including solvency effects, in a colloid−polymer mixture is essential for a quantitative theoretical description of the colloidal gas−liquid interface. The commonly used penetrable hard sphere model yields an unphysical description of the colloidal gas−liquid interface, even though the bulk phase behavior is often quite reasonable. Our measurements are in accordance with a Gaussian-like diffuseness of the interface; that is, we observe no evidence for layering or oscillations in the density profiles. Future research may be directed at probing systematically the effect of varying the range of the interactions, the influence of other interactions, and the role of thermal capillary waves. We expect that X-ray reflectivity and similarly neutron reflectivity can be valuable tools for studying other types of interfaces[26] in soft matter systems.

■ ASSOCIATED CONTENT

Supporting Information

The Supporting Information is available free of charge at https://pubs.acs.org/doi/10.1021/acs.jpclett.0c02464.

Description of materials, details regarding X-ray reflectivity measurements, and additional expressions and results from free-volume theory (PDF)

■ AUTHOR INFORMATION

Corresponding Author

Mark Vis − *Laboratory of Physical Chemistry, Department of Chemical Engineering and Chemistry and Institute for Complex Molecular Systems, Eindhoven University of Technology, 5600 MB Eindhoven, The Netherlands;* orcid.org/0000-0002-2992-1175; Email: m.vis@tue.nl

Authors

Kelly J. H. Brouwer − *Laboratory of Physical Chemistry, Department of Chemical Engineering and Chemistry and Institute for Complex Molecular Systems, Eindhoven University of Technology, 5600 MB Eindhoven, The Netherlands; Van 't Hoff Laboratory for Physical and Colloid Chemistry, Debye Institute for Nanomaterials Science, Utrecht University, 3508 TA Utrecht, The Netherlands*

Álvaro González García − *Van 't Hoff Laboratory for Physical and Colloid Chemistry, Debye Institute for Nanomaterials Science, Utrecht University, 3508 TA Utrecht, The Netherlands; Laboratory of Physical Chemistry, Department of Chemical Engineering and Chemistry and Institute for Complex Molecular Systems, Eindhoven University of Technology, 5600 MB Eindhoven, The Netherlands;* orcid.org/0000-0002-5343-1467

Andrei V. Petukhov − *Van 't Hoff Laboratory for Physical and Colloid Chemistry, Debye Institute for Nanomaterials Science, Utrecht University, 3508 TA Utrecht, The Netherlands; Laboratory of Physical Chemistry, Department of Chemical Engineering and Chemistry, Eindhoven University of Technology, 5600 MB Eindhoven, The Netherlands;* orcid.org/0000-0001-9840-6014

Oleg Konovalov − *European Synchroton Radiation Facility, 38000 Grenoble, France*

Remco Tuinier − *Laboratory of Physical Chemistry, Department of Chemical Engineering and Chemistry and Institute for Complex Molecular Systems, Eindhoven University of Technology, 5600 MB Eindhoven, The Netherlands;* orcid.org/0000-0002-4096-7107

Complete contact information is available at: https://pubs.acs.org/10.1021/acs.jpclett.0c02464

Notes

The authors declare no competing financial interest.

■ ACKNOWLEDGMENTS

The authors acknowledge the European Synchrotron Radiation Facility for the granted beamtime on beamline ID10. M.V. acknowledges The Netherlands Organisation for Scientfic Research (NWO) for a Veni Grant (722.017.005) and Dr. Edgar Blokhuis for insightful discussions. Substantial portions of this Letter were written during a research stay by M.V. at Laboratoire de Chimie, École Normale Supérieure de Lyon (Lyon, France); M.V. thanks Prof. M. F. Costa Gomes and Prof. A. A. H. Pádua for their hospitality. The authors acknowledge S. J. Oosterink (Equipment & Prototype Center, TU/e) for designing and manufacturing the X-ray sample cells. The authors acknowledge J. Opdam for measurement of the phase diagram.

■ REFERENCES

(1) Alder, B. J.; Wainwright, T. E. Phase transition for a hard sphere system. *J. Chem. Phys.* **1957**, *27*, 1208−1209.

(2) Wood, W. W.; Jacobson, J. D. Preliminary results from a recalculation of the monte carlo equation of state of hard spheres. *J. Chem. Phys.* **1957**, *27*, 1207−1208.

(3) Pusey, P. N.; van Megen, W. Phase behaviour of concentrated suspensions of nearly hard colloidal spheres. *Nature* **1986**, *320*, 340−342.

(4) Poon, W. C. K. Colloids as big atoms. *Science* **2004**, *304*, 830−831.

(5) Dijkstra, M. Entropy-Driven Phase Transitions in Colloids: From Spheres to Anisotropic Particles. *Adv. Chem. Phys.* **2014**, *156*, 35−71.

(6) Evans, R.; Frenkel, D.; Dijkstra, M. From simple liquids to colloids and soft matter. *Phys. Today* **2019**, *72*, 38.

(7) Poon, W. C.-K. The physics of a model colloid-polymer mixture. *J. Phys.: Condens. Matter* **2002**, *14*, R859−R880.

(8) Asakura, S.; Oosawa, F. On interaction between two bodies immersed in a solution of macromolecules. *J. Chem. Phys.* **1954**, *22*, 1255−1256.

(9) Asakura, S.; Oosawa, F. Interaction between particles suspended in solutions of macromolecules. *J. Polym. Sci.* **1958**, *33*, 183−192.
(10) Vrij, A. Polymers at interfaces and the interactions in colloidal dispersions. *Pure Appl. Chem.* **1976**, *48*, 471−483.
(11) Lekkerkerker, H. N. W.; Tuinier, R. *Colloids and the Depletion Interaction*; Lecture Notes in Physics *833*; Springer, 2011.
(12) Lekkerkerker, H. N. W.; Poon, W. C.-K.; Pusey, P. N.; Stroobants, A.; Warren, P. B. Phase-behavior of colloid plus polymer mixtures. *Europhys. Lett.* **1992**, *20*, 559−564.
(13) Ilett, S. M.; Orrock, A.; Poon, W. C. K.; Pusey, P. N. Phase behavior of a model colloid-polymer mixture. *Phys. Rev. E: Stat. Phys., Plasmas, Fluids, Relat. Interdiscip. Top.* **1995**, *51*, 1344−1352.
(14) Frenkel, D. Playing tricks with designer "atoms. *Science* **2002**, *296*, 65−66.
(15) Dickinson, E. Colloid science of mixed ingredients. *Soft Matter* **2006**, *2*, 642−652.
(16) Dickinson, E. *Colloids in Paints*; Wiley-VCH, 2011.
(17) Doublier, J.-L.; Garnier, C.; Renard, D.; Sanchez, C. Protein−polysaccharide interactions. *Curr. Opin. Colloid Interface Sci.* **2000**, *5*, 202−214.
(18) Saunders, B. R.; Turner, M. L. Nanoparticle−polymer photovoltaic cells. *Adv. Colloid Interface Sci.* **2008**, *138*, 1−23.
(19) Syrbe, A.; Bauer, W.; Klostermeyer, H. Polymer science concepts in dairy systems—an overview of milk protein and food hydrocolloid interaction. *Int. Dairy J.* **1998**, *8*, 179−193.
(20) Aarts, D. G. A. L. The interface in demixed colloid−polymer systems: wetting, waves and droplets. *Soft Matter* **2007**, *3*, 19−23.
(21) Vink, R. L. C.; Horbach, J.; Binder, K. Capillary waves in a colloid-polymer interface. *J. Chem. Phys.* **2005**, *122*, 134905−12.
(22) Blokhuis, E. M.; Kuipers, J.; Vink, R. L. C. Description of the fluctuating colloid-polymer interface. *Phys. Rev. Lett.* **2008**, *101*, No. 086101.
(23) Fortini, A.; Dijkstra, M.; Schmidt, M.; Wessels, P. P. F. Wall-fluid and liquid-gas interfaces of model colloid-polymer mixtures by simulation and theory. *Phys. Rev. E* **2005**, *71*, 051403.
(24) Aarts, D. G. A. L.; Schmidt, M.; Lekkerkerker, H. N. W. Direct visual observation of thermal capillary waves. *Science* **2004**, *304*, 847−850.
(25) Vis, M.; Peters, V. F. D.; Blokhuis, E. M.; Lekkerkerker, H. N. W.; Erné, B. H.; Tromp, R. H. Decreased interfacial tension of demixed aqueous polymer solutions due to charge. *Phys. Rev. Lett.* **2015**, *115*, No. 078303.
(26) Chao, Y.; Shum, H. C. Emerging aqueous two-phase systems: from fundamentals of interfaces to biomedical applications. *Chem. Soc. Rev.* **2020**, *49*, 114−142.
(27) Brader, J. M.; Evans, R. The fluid-fluid interface of a model colloid-polymer mixture. *Europhys. Lett.* **2000**, *49*, 678−684.
(28) Brader, J. M.; Evans, R.; Schmidt, M.; Löwen, H. Entropic wetting and the fluid-fluid interface of a model colloid-polymer mixture. *J. Phys.: Condens. Matter* **2002**, *14*, L1−L8.
(29) Magnussen, O. M.; Ocko, B. M.; Regan, M. J.; Penanen, K.; Pershan, P. S.; Deutsch, M. X-ray reflectivity measurements of surface layering in liquid mercury. *Phys. Rev. Lett.* **1995**, *74*, 4444−4447.
(30) de Hoog, E. H. A.; Lekkerkerker, H. N. W.; Schulz, J.; Findenegg, G. H. Ellipsometric study of the liquid/liquid interface in a phase-separated colloid−polymer suspension. *J. Phys. Chem. B* **1999**, *103*, 10657−10660.
(31) Royall, C. P.; Aarts, D. G. A. L.; Tanaka, H. Bridging length scales in colloidal liquids and interfaces from near-critical divergence to single particles. *Nat. Phys.* **2007**, *3*, 636.
(32) van Helden, A. K.; Jansen, J. W.; Vrij, A. Preparation and characterization of spherical monodisperse silica dispersions in nonaqueous solvents. *J. Colloid Interface Sci.* **1981**, *81*, 354−368.
(33) Pathmamanoharan, C.; Philipse, A. P. Preparation of small alkane-grafted silica particles (for SAXS and SANS studies) from aqueous commercial sols. *J. Colloid Interface Sci.* **1994**, *165*, 519−521.
(34) de Hek, H.; Vrij, A. Interactions in mixtures of colloidal silica spheres and polystyrene molecules in cyclohexane I. phase separations. *J. Colloid Interface Sci.* **1981**, *84*, 409−422.
(35) van Helden, A. K.; Vrij, A. Static light scattering of concentrated silica dispersions in apolar solvents. *J. Colloid Interface Sci.* **1980**, *78*, 312−329.
(36) Smilgies, D.-M.; Boudet, N.; Struth, B.; Konovalov, O. Troika ii: a versatile beamline for the study of liquid and solid interfaces. *J. Synchrotron Radiat.* **2005**, *12*, 329−339.
(37) It should be stressed that the concentrations mentioned are only indicative, as cyclohexane is highly volatile; an uncertainty of about 10% is to be expected.
(38) *X-ray and Neutron Reflectivity: Principles and Applications*; Daillant, J., Gibaud, A., Eds.; Lecture Notes in Physics *770*; Springer, 2009.
(39) Bodnár, I.; Oosterbaan, W. D. Indirect determination of the composition of the coexisting phases in a demixed colloid polymer mixture. *J. Chem. Phys.* **1997**, *106*, 7777−7780.
(40) Fleer, G. J.; Tuinier, R. Analytical phase diagrams for colloids and non-adsorbing polymer. *Adv. Colloid Interface Sci.* **2008**, *143*, 1−47.
(41) Rowlinson, J. S.; Widom, B. *Molecular Theory of Capillarity*; Dover Publications, 1982.
(42) Aarts, D. G. A. L.; Dullens, R. P. A.; Lekkerkerker, H. N. W.; Bonn, D.; van Roij, R. Interfacial tension and wetting in colloid−polymer mixtures. *J. Chem. Phys.* **2004**, *120*, 1973−1980.
(43) Carnahan, N. F.; Starling, K. E. Equation of state for nonattracting rigid spheres. *J. Chem. Phys.* **1969**, *51*, 635−636.
(44) Fleer, G. J.; Tuinier, R. The critical endpoint in phase diagrams of attractive hard spheres. *Phys. A* **2007**, *379*, 52−58.
(45) This effect is reduced for the good solvent and theta solvent models, since the compression of depletion zones at higher polymer concentrations reduces the range of attractions and lowers the triple point.
(46) Blokhuis, E. M.; Bedeaux, D. Optical properties of the fluid-fluid interface. *Phys. A* **1990**, *164*, 515−548.
(47) Binder, K.; Virnau, P.; Statt, A. Perspective: the Asakura Oosawa model: a colloid prototype for bulk and interfacial phase behavior. *J. Chem. Phys.* **2014**, *141*, 140901.
(48) Brader, J. M.; Evans, R.; Schmidt, M. Statistical mechanics of inhomogeneous model colloid−polymer mixtures. *Mol. Phys.* **2003**, *101*, 3349−3384.

https://dx.doi.org/10.1021/acs.jpclett.0c02464
J. Phys. Chem. Lett. 2020, 11, 8372−8377